Materials Advances

ROYAL SOCIETY OF CHEMISTRY

PAPER

View Article Online
View Journal | View Issue

Cite this: *Mater. Adv.*, 2025, 6, 1392

A stretchable PVA–agar hydrogel patch embedded with metal-doped carbon dots (MCD) for monitoring the Ca^{2+} biomarker†

Lingaraj Behera[a] and Sasmita Mohapatra *[ab]

Received 17th September 2024,
Accepted 6th January 2025

DOI: 10.1039/d4ma00935e

rsc.li/materials-advances

Calcium ions play a vital role in skeletal growth, muscle action and neural signalling. Thus, the level of calcium in the body is a crucial parameter in the diagnosis of muscle weakness and osteoporosis. Fluorescence conductive hydrogels are widely employed in electronic devices as they are able to monitor single or multiple parameters in synergistic optical and electrical modes. However, integrating optical and conductive modalities and synergizing their various functions to develop a wearable sensor is challenging. In this regard, a PVA–agar hydrogel (PAGH) cross-linked with copper-doped carbon dot (MCD) was fabricated. The developed MCD@PAGH addressed Ca^{2+} recognition through a change in ionic conductance and fluorescence. The hydrogel patch sensor was not cytotoxic, exhibited bactericidal activity, and monitored Ca^{2+} level in sweat in both the fluorescence and electrical modes. This work provides a strategy to design multifunctional materials to address prospective applications in wearable biosensors.

1. Introduction

In the current intelligent era, the increasing demand for higher work efficiency and comfortable daily life has motivated research on wearable sensors. In the past few years, these sensors have gained great attention owing to their ability to detect real time physiological parameters, such as metabolites (urea, lactate), electrolytes (Na^+, K^+, Mg^{2+}, Cl^-, Ca^{2+}), heavy metals and proteins.[1–3] Particularly, user-friendly electronic sensors with optical components that promote the visualization of one or more physiological parameters have garnered much attention recently.[4] Such type of multifunctional sensors hold potential to present symbolic information as well as electrical signals, which contribute towards the real-time monitoring of health parameters during physical movement.[5] Designing such optoelectronic sensors is challenging and demands synergetic uniform distribution of different functional components in the sensor matrix.

On the other hand, the chemical composition of sweat dynamically reflects the levels of various biomarkers that pertain to the physiological changes in the human body.[6,7] Among various biomarkers, Ca^{2+} is an essential electrolyte. Its concentration in sweat varies in the range from 0.2 to 2.0 mol L^{-1}. Ca^{2+} abnormalities can cause severe muscle and nerve tightness and various pathological disorders.[8,9] During expansion and contraction coupling in skeletal muscles, Ca^{2+} ions are released into the myoplasm by the sarcoplasmic reticulum in response to the depolarization of the transverse T-membrane. Therefore, accurate determination of Ca^{2+} holds great promise for health monitoring.[10]

Skin-adhesiveness, flexibility and super-biocompatibility are three important factors to consider while developing a wearable sensor.[11] For this purpose, conductive hydrogels constituting 3D crosslinked network with good water absorbing capacity have been accepted as extremely suitable materials to design wearable sensors because of their tissue-like properties. Post-synthesis treatment of rigid conductive polymers with water soluble polymers is an effective strategy to improve the mechanical as well as conductive nature of the polymer gel.[12,13] In another way, conductive polymer hydrogels can be developed by incorporating multivalent metal ions, nanomaterials, carbon nanotube, and graphene/reduced graphene oxide as fillers into the polymer matrix.[14] For instance, Li and his coworkers synthesized a flexible wearable electrochemical sensor using the MXene–hydrogel composite for monitoring glucose in sweat.[15] Wang *et al.* synthesized a flexible, adhesive PVA/sucrose hydrogel patch for colorimetric sweat monitoring to enable convenient and personalized point-of-care detection.[16] A stable hydrogel network was constructed from cellulose nanocrystals and PVA film, which can adsorb sodium alginate and act as a selective and sensitive

[a] *Department of Chemistry, National Institute of Technology Rourkela, Odisha, 769008, India. E-mail: sasmitam@nitrkl.ac.in*
[b] *Centre for Nanomaterials, National Institute of Technology Rourkela, Odisha, 769008, India*

† Electronic supplementary information (ESI) available. See DOI: https://doi.org/10.1039/d4ma00935e

sensor for detecting Ca^{2+} ions in sweat.[17] Sun *et al.* developed a supramolecular conductive hydrogel with exceptional anti-swelling properties by incorporating polypyrrole into polyacrylamide and/or sodium alginate solution.[18] This hydrogel patch could have been applied to sense body motion underwater. From a functional design perspective, adding different recognition units while keeping the conductive and mechanical properties intact should be the main objective while designing a wearable sensor for monitoring Ca^{2+} ion concentration.

In this work, we have rationally developed a stretchable and adhesive wearable hydrogel patch to collect information on the concentration of Ca^{2+} through fluorescence as well as electrochemical signal detection. An adhesive conductive hydrogel was developed by intermixing optimized amounts of PVA and agar. Agar is a biological polysaccharide with good biocompatibility and multiple –OH groups, providing potential H-bonds with PVA chains.[19] Furthermore, the solubility of agar in water and the interactions between them could be easily tuned by temperatures and ion concentrations.[20] PVA chains were used as the soft filler to provide flexibility and mechanical strength to the hydrogel. Additionally, we incorporated fluorescent hydrophilic copper-doped carbon dot (MCD) into PVA–agar hydrogel (PAGH) during intermixing to impart enhanced mechanical strength as well as Ca^{2+} specific recognition to the hydrogel through fluorescence (FL) and conductance. The resulting MCD@PAGH shows multiple advantages: (1) the uniform distribution of hydrophilic MCD enhances crosslinking and hence mechanical strength, (2) good resilience and self-healing, (3) selectively senses Ca^{2+} in sweat through fluorescence and electrochemical dual response during various physical activities due to the specific chemical interaction of Ca^{2+} with MCD. To the best of our knowledge, this is the first report on the design of a skin adhesive hydrogel for monitoring Ca^{2+} in the dual mode and may be explored as a wearable sensor for health monitoring.

2. Experimental

2.1. Reagents

Ethylenediaminetetraacetic acid (EDTA) and citric acid (CA) were brought from Sigma-Aldrich. Calcium chloride ($CaCl_2$) and other chemicals were brought from Fischer Chemical Pvt Ltd. NH_4OH, NaOH, NaCl, KCl, and $MgCl_2$ were obtained from Lobachemie Pvt. Ltd, India. Polyvinyl alcohol (PVA) and agar were purchased from HIMEDIA. To measure the pH of the solution, we prepared phosphate-buffered saline (PBS) solutions with various pH values utilising 0.1 mol L^{-1} of HCl and 0.1 mol L^{-1} of NaOH.

2.2. Fabrication of MCD@PAGH

MCD was prepared from citric acid EDTA and $CuCl_2$ following the procedure recently published from our laboratory.[21] For the synthesis of copper-doped carbon dot-incorporated PVA–agar hydrogel (MCD@PAGH), 6 g of PVA and 1.5 g of agar were mixed in 60 mL of double distilled water until the mixed solution was completely homogenous. To completely dissolve PVA and agar, the resultant solution was heated at 90 °C for 1 h. Then, MCD solution (2 mg mL^{-1}) was added to the transparent PVA–agar solution in the beaker and stirred for 30 min till MCD was completely miscible inside the PVA–agar gel solution. After that, the solution mixture was poured into a mold with an inner diameter of 24 mm and height of 11 mm and then allowed to cool at 25 °C. In the end, the gel mold was made through the repeatedly freezing and thawing treatment (4 times, −20 °C to RT, 24 h every time). Meanwhile, following the above process, 0.5 mg mL^{-1}, 2 mg mL^{-1}, and 4 mg mL^{-1} of MCD solution were mixed prior to the PVA–agar gel solution and designated as MCD@PAGH 0.5, MCD@PAGH 2, and MCD@PAGH 4, respectively. The synthesis process of MCD@PAGH was optimized by examining the effects of PVA amount, agar and MCD. All the raw material ratios and optimization process for hydrogel synthesis are mentioned in the ESI† (Table S1).

2.3. Characterization of MCD and MCD@PAGH

The experimental techniques followed for the characterization of MCD and MCD@PAGH have been explained in the ESI† (Fig. S1, S3, S4 and S8).

2.4. Fluorescence detection of Ca^{2+} in solution and using MCD@PAGH

The fluorescence response of the MCD towards Ca^{2+} was recorded using a spectrofluorometer. The details of sensing conditions and protocol has been described in ESI.† The fluorescence responses of MCD@PAGH patch towards Ca^{2+} were measured by adding Ca^{2+} solution (50–300 μM, 1 mL) to the patch and the FL emission intensity was monitored under a UV lamp. The image was analysed using ImageJ software. The R (red), G (green), and B (blue) values of the hydrogel sample were recorded using the RGB app in the smartphone. The amount of Ca^{2+} in real sweat samples was explored following the similar experimental protocol (ESI†).

2.5. Detection of Ca^{2+} through the electrochemical (EC) study

A small piece of MCD@PAGH measuring 15 mm in height and 10 mm in width was cut from a larger hydrogel with a diameter of 55 mm and placed between two specially made Teflon modules. Ionic currents across the membrane were measured with a Keithley 6487 picoammeter. A pair of Au probes was subjected to a voltage sweep ranging from −5 to +5 V, with a step size of 0.25 V. The ionic current of PAGH was indexed as the initial current value. Next, different amounts of analyte solutions, which included various calcium ions and other anions and cations, were added to the PAGH. Before each test, solutions of the analyte were added drop by drop to the PAGH patch, and the ionic currents were measured after 10 minutes of absorption. The practical application of MCD@PAGH patch in the EC sensing of Ca^{2+} in real sweat samples was explored on volunteers during the commencement of certain physical activities.

2.6. Antibacterial activity of MCD@PAGH

The antibacterial activity was studied using *Escherichia coli* (E.C.), a type of Gram-negative bacteria, and *Staphylococcus aureus* (S.A.), a type of Gram-positive bacteria. The bacterial

strains were transferred from a −20 °C freezer onto agar plates and cultured in nutrient agar for 12 h at 37 °C. Individual bacterial colonies were collected from agar plates and incubated in MHB (Mueller Hinton agar) medium at 37 °C for 6–8 h. Next, 100 μL of bacteria suspension was added to only MHB and MHB-containing PAGH, MCD@PAGH 0.5, MCD@PAGH 2, and MCD@PAGH 4. The samples were placed inside an incubator shaker at 37 °C and kept overnight. 100 μL of 5-fold diluted bacterial suspension from each sample sets were spread on and agar plate and incubated overnight for bacterial growth. To measure the antibacterial activity of the fabricated hydrogels, the colony forming units' (CFU) calculation method was considered. The photographs of the agar plates were taken, and the formed bacterial colony was calculated using the following formula.

$$\text{Survival rate } (\%) = \frac{\text{CFU}_x}{\text{CFU}_0} \times 100 \quad (1)$$

where $(\text{CFU})_x$ is the colony forming unit of the hydrogel-treated bacteria and $(\text{CFU})_0$ is the unreacted bacterial colony count.

2.7. Cytotoxicity

MTT(3-(4,5-dimethylthiazol-2-yl)-2,5-diphenyltetrazolium bromide) method was employed to investigate the cytotoxicity of MCD@PAGH 2 on the LN229 glioblastoma cell line. In the MTT study, 3×10^3 cells were plated in 96-well plates at a uniform density using 100 μL complete growth media and allowed to adhere overnight. The cells were washed with PBS before being placed in fresh culture media that contained different amounts of MCD@PAGH 2 (10, 25, 50, 75, 100 μg mL^{-1}). After 24 h incubation, the treated cells were rinsed with 200 μL of PBS, and then 100 μL of MTT solution (0.5 mg mL^{-1}) was mixed in each well. Next, the plates were kept in an incubator for 4 h at 37 °C with 80% relative humidity and 5% CO_2. The UV absorbance of each well was measured at 590 nm using a UV-vis plate reader (PerkinElmer, VICTOR x3). All experiments were conducted three times and repeated at least twice. The extract solution was analyzed using confocal laser scanning microscopy (CLSM).

3. Results and discussion

3.1. Design principles and characterization of MCD@PAGH

In the case of hydrogels, agar was selected as a substrate due to its excellent biocompatibility and the abundance of hydroxyl (–OH) groups, which can form strong hydrogen bonds with PVA (polyvinyl alcohol) and MCD (Scheme 1). PVA contributes sufficient mechanical strength to the hydrogel. Additionally, the enhancement of charge carrier delocalization through hydrogen bonding leads to an increase in electrical conductivity. The synergistic crosslinking chemistry resulted in the construction of MCD@PAGH (MCD-loaded PVA–agar hydrogel).[22]

Agar molecules contain hydrogen atoms that can function as both hydrogen bond donors and acceptors. When combined with PVA chains, agar creates numerous hydrogen bonds with the –OH groups on the PVA chains, acting as a cross-linker. Furthermore, secondary cross-linking occurs during the repeated freeze–thawing process, which increases the stability of the hydrogel. The inclusion of MCD further enhances cross-linking, as indicated by the gelation time. The gelation time for the PVA–agar hydrogel was approximately 60 minutes. However, with the addition of MCD,

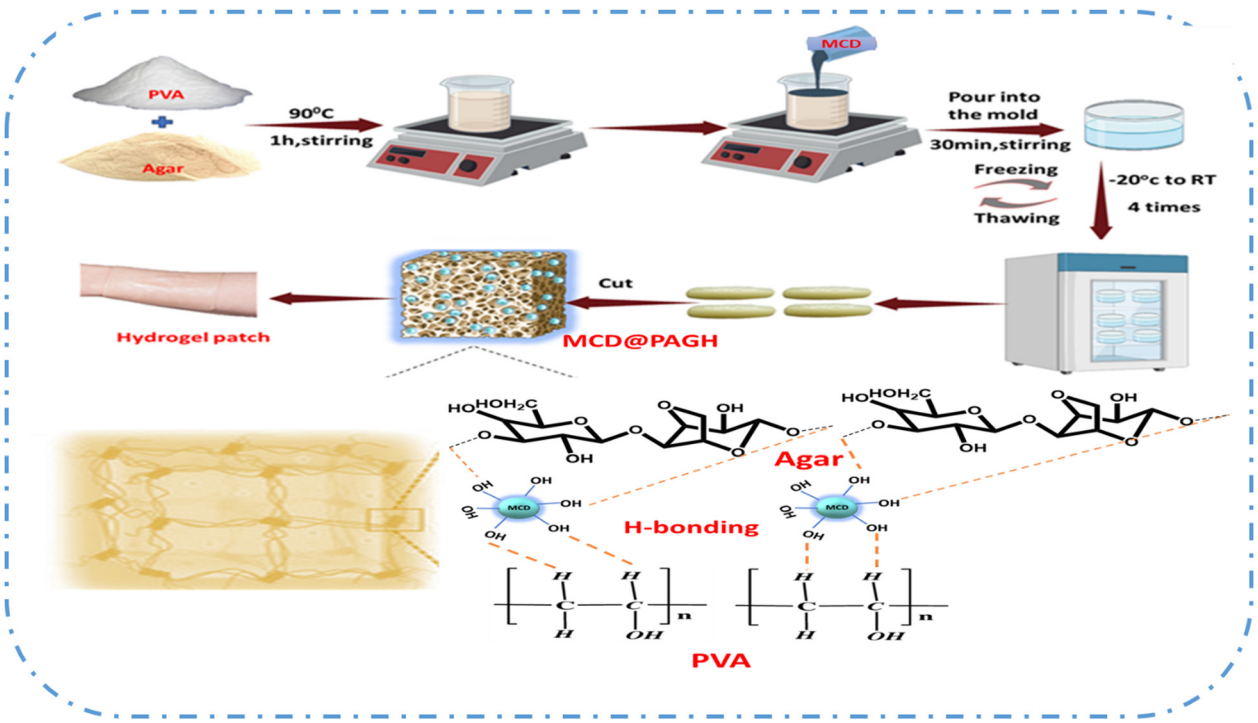

Scheme 1 Illustration of the synthesis of MCD@PAGH.

this time reduces significantly. Specifically, the gelation time for the PVA–agar hydrogel decreased from 20 to 10 minutes as the concentration of MCD increased from 0.5 to 4 mg mL^{-1}. This reduction can be attributed to the increased cross-linking between the polymers due to the higher concentration of MCD, resulting in faster gelation. The hydrogel displays an intricate cross-linking system that includes chemical cross-linking, ionic cross-linking, and hydrogen bond interactions. The hydroxyl-rich chains capture water molecules, facilitating ion migration and enhancing the sensitivity of MCDs to Ca^{2+} stimulation. MCD plays a crucial role in the PAGH network as its skeletal adhesion determines the overall emission color of the hydrogel.

The optical pictures in Fig. 1a displayed that MCD@PAGH sample is a translucent gel ($T = 13\%$) and light brown in colour. In the SEM (scanning electron microscope) images of the PAGH and MCD@PAGH (Fig. 1b–e), the as-synthesized PAGH shows a denser interconnected porous network structure, which confirms the strong hydrogen bonding between PVA and agar. The SEM images of the lyophilized specimen of PAGH with varying percentages of agar is shown in Fig. S3a–f (ESI†). The hydrogel stable 3D network structure was observed in the SEM image, which showed the presence of numerous micropores and mesopores within the PAGH. The staggered pore structure allows for the easy intake of MCD. As the MCD content increases, the pore size in the hydrogel decreases gradually. The intense cross-linking between MCD, agar, and PVA enhances the stability of the hydrogel, resulting in a denser gel structure. The detailed pore size distributions of the optimized PAGH and MCD@PAGH are explained in ESI.† As mentioned in Table S2 (ESI†), MCD@PAGH 4 has the lowest pore size, suggesting that the hydrogel's internal network becomes more compact with higher MCD content. EDX (energy-dispersive X-ray spectroscopy) analysis shows the presence of copper (Cu), carbon (C), nitrogen (N), and oxygen (O). Cu is evenly distributed in the composite hydrogel.

The interaction between the PVA polymer chains and loaded MCDs under gel-forming conditions were established by FTIR (Fourier transform infrared spectroscopy). PVA displays peaks at 1094, 1427 and 3375 cm^{-1} for C–O, C–H and O–H stretching, respectively.[23] Compared to the starting polymer, the O–H stretching vibration in PAGH shifts to 3322 cm^{-1}, showing the formation of a hydrogen bond.[24] After MCD was loaded into the PAGH, the peak at about 980–670 cm^{-1} is ascribed to Cu–OH stretching vibration and the vibrational, frequency varies with degree of hydrogen bonding, which confirms the crosslinking between metal (copper) and hydroxyl group present in the hydrogel (Fig. 1f). The effect of hydrogel formation and binding efficiency of MCD inside the hydrogel were analysed using XPS (X-ray photoelectron spectroscopy). As mentioned in Fig. S5a–e (ESI†), the XPS survey spectrum of MCD@PAGH shows C 1s, N 1s, O 1s, and Cu 2p peaks, indicating that hydrogel synthesis has a limited effect on the carbon dots. The high-resolution XPS spectra can be deconvoluted into Cu $2p_{1/2}$ and Cu $2p_{3/2}$ with three additional satellite peaks situated at 962.1, 943.3 and 941.2 eV. These extra peaks are commonly a result of the "shake up" phenomenon triggered by the stimulation of excess electrons to higher energy levels. The Cu $2p_{1/2}$ peak can be deconvoluted into two peaks at

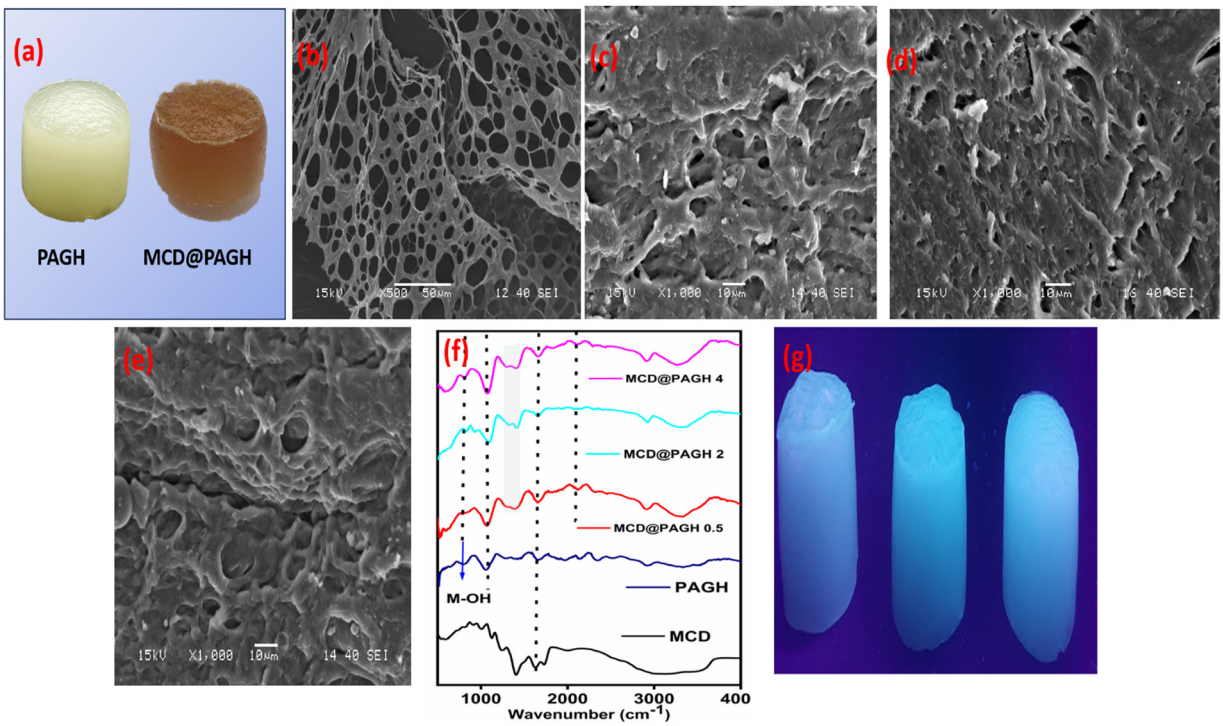

Fig. 1 (a) PAGH and MCD@PAGH structure visible with naked eye, SEM image of (b) PAGH, (c) MCD@PAGH 0.5, (d) MCD@PAGH 2, (e) MCD@PAGH 4, (f) FTIR spectra of PAGH and MCD@PAGH, (g) MCD@PAGH image under UV light.

952.8 and 954.9 eV, which are indexed to Cu^0 and Cu^{2+}, respectively.[25] The Cu $2p_{3/2}$ peak can be divided into two peaks at 932.6 and 934.8 eV assigned to Cu^0 and Cu^{2+}, respectively.[26] In addition, XPS results proved that Cu^{2+} forms good coordination with the carboxylic group. The C–O binding energy in PAGH without Cu is 533.1 eV, whereas the binding energy of C–O in MCD@PAGH is 533.5 eV. This shows that oxygen binding energy increased by 0.4 eV after Cu^{2+} coordinated with the carboxyl group, causing the peak to shift slightly to the right. This result shows that Cu^{2+} has good metal coordination with PAGH. The high-resolution scan of C 1s deconvoluted into three peaks at 285.9, 284.7, and 288.6 eV, which may be indexed to C–O/C–N, C═C, and C═O, respectively.[27] The N 1s high-resolution scan shows two sharp peaks at 401.8 and 399.8 eV ascribed to pyrrolic and pyridinic nitrogen, respectively.[28] The slight shift of peaks in the MCD@PAGH as compared to PAGH could be attributed to the interaction between MCD and PAGH. Furthermore, the presence of MCD particulates significantly enhanced the development of a conductive 3D network structure within the hydrogel. This network structure played a vital role for enhancing both the mechanical and electrical characteristics of MCD@PAGH, which will provide its great potential for expanding applications in artificial intelligence (AI) and wearable strain sensors.

3.2. Optical properties of MCD and MCD@PAGH

The optical properties of MCD were studied by analysing the UV-vis absorption and emission spectra (Fig. S6a, ESI†). An intense absorption peak at 223 nm indicates the $\pi \rightarrow \pi^*$ electronic shift of the graphitic carbon core, with a tail that stretches into the visible region.[29] As mentioned earlier, MCD shows intense blue colour under UV light; thus, it was observed that MCD@PAGH emits cyan blue colour fluorescence under a UV lamp (Fig. 1g). The FL behaviours of MCD were also examined by raising the excitation-dependent wavelength from 330 to 410 nm with 10 nm steps. As mentioned in Fig. S6b (ESI†), MCD shows an excitation-dependent FL emission behaviour due to various energy traps in the CD (carbon dot). The FL emission peak at 445 nm was due to the π–π^* transitions in the sp^2-hybridized carbon core and the n–π^* excitations attributed to the surface-related defect states resulting from metal atom doping. MCDs had greater emission intensity than CD and its quantum yield (QY) was found to be 15.27% higher than that of CDs (Fig. S6c, ESI†). The FL stability of MCDs at various pH levels was assessed. As shown in Fig. S6d (ESI†), the pH had no notable impact on the FL intensity. The highest FL intensity of MCDs was shown at pH 8, while it slightly decreased under highly acidic conditions. In a highly acidic environment, all –COOH groups on the surface of MCD become protonated. However, under strongly alkaline conditions, the concentration of calcium ions can be significantly affected. In an alkaline environment, all –COOH groups on the surface of MCD remain as anions, which is perfect for coordinating Ca^{2+} ions and forming octahedral complexes. However, in between pH 6 and 8, there was significant quenching of the fluorescence intensity of MCD due to coordination with Ca^{2+} (Fig. S6e, ESI†). Thus, it indicates that the developed hydrogel patch can be used to detect Ca^{2+} in sweat where the pH was 6.3. Additionally, the long-term stability of the MCDs was assessed. The MCDs demonstrated exceptional durability, as evidenced by a minimal 9% decrease in the fluorescence intensity after being stored for 10 days (Fig. S6f, ESI†).

3.3. Mechanical properties of MCD@PAGH

It is expected that the incorporation of MCD with ample hydrophilic surface functional groups may induce crosslinking and hence improve the mechanical property of MCD@PAGH. A comparison of the mechanical properties of MCD@PAGH and PAGH shows that the stretching of MCD@PAGH succeeded over PAGH (Fig. 2a). MCD@PAGH is highly flexible and endures high level deformation, which arises due to normal and twisted stretching (Fig. 2a). An MCD@PAGH cylindrical string could sustain after bearing 100–600 g load without breaking. Additionally, MCD@PAGH tolerates heavy compression and comes back to the original shape after withdrawing the compression force (Fig. 2b), which implies that the hydrogel has good resilience property. At the same time, the as-prepared PAGH showed poor recovery. To investigate the mechanical properties in detail, compressive and tensile tests were done. The tensile stress vs strain plots of the MCD@PAGH with different MCD contents (Fig. 2c) and their respective toughness are illustrated in Fig. 2d. It can be interpreted that the tensile properties of MCD@PAGH are noticeably superior than that of PAGH. Also, the stretchability of MCD@PAGH is finely controlled by the MCD content. PAGH showed tensile stress, fracture strain and toughness of 0.043 MPa, 121% and 0.50 MJ m^{-3}, respectively, whereas with the addition of 2 mg mL^{-1} MCD, the tensile strength, toughness and fracture strain were significantly enhanced to 0.149 MPa, 3.79 MJ m^{-3} and 164%, respectively. The good dispersion of MCD with abundant hydrophilic functional groups in the hydrogel network could be the main reason behind high mechanical strength and superior stretchability. This MCD acts as a nano-filler, which greatly reinforces the PAGH due to the nanofiller-induced reinforcement effect.[30] At the same time, the functional surface of MCDs offers physical cross-linking sites *via* strong hydrogen bonding interactions between the PAG parts and MCD, which effectively distributes the deformation energy, toughening the whole hydrogels, which is evidenced by the modulus analysis. The Young's modulus of PAGH gradually increases with an increase in the MCD content and at higher concentration of MCD modulus, it decreases due to high cross-linking. However, with higher MCD, the mechanical parameters were decreased, which might be due to the formation of MCD aggregates.[31] Similarly, the analysis of compression mechanical properties was done by plotting stress–strain plots and compression strength at 73% strain of MCD@PAGH with different MCD contents (Fig. 2e and f). As compared to similar materials, the developed MCD@PAGH shows good tensile properties (Movies S1, S2 and Table S3, ESI†). Furthermore, the Young's modulus and fracture energy of MCD@PAGH 2 are much higher than that of PAGH (Fig. S7a–c, ESI†). The higher deformability and toughness stem from the reversible interactions between PVA and agar,

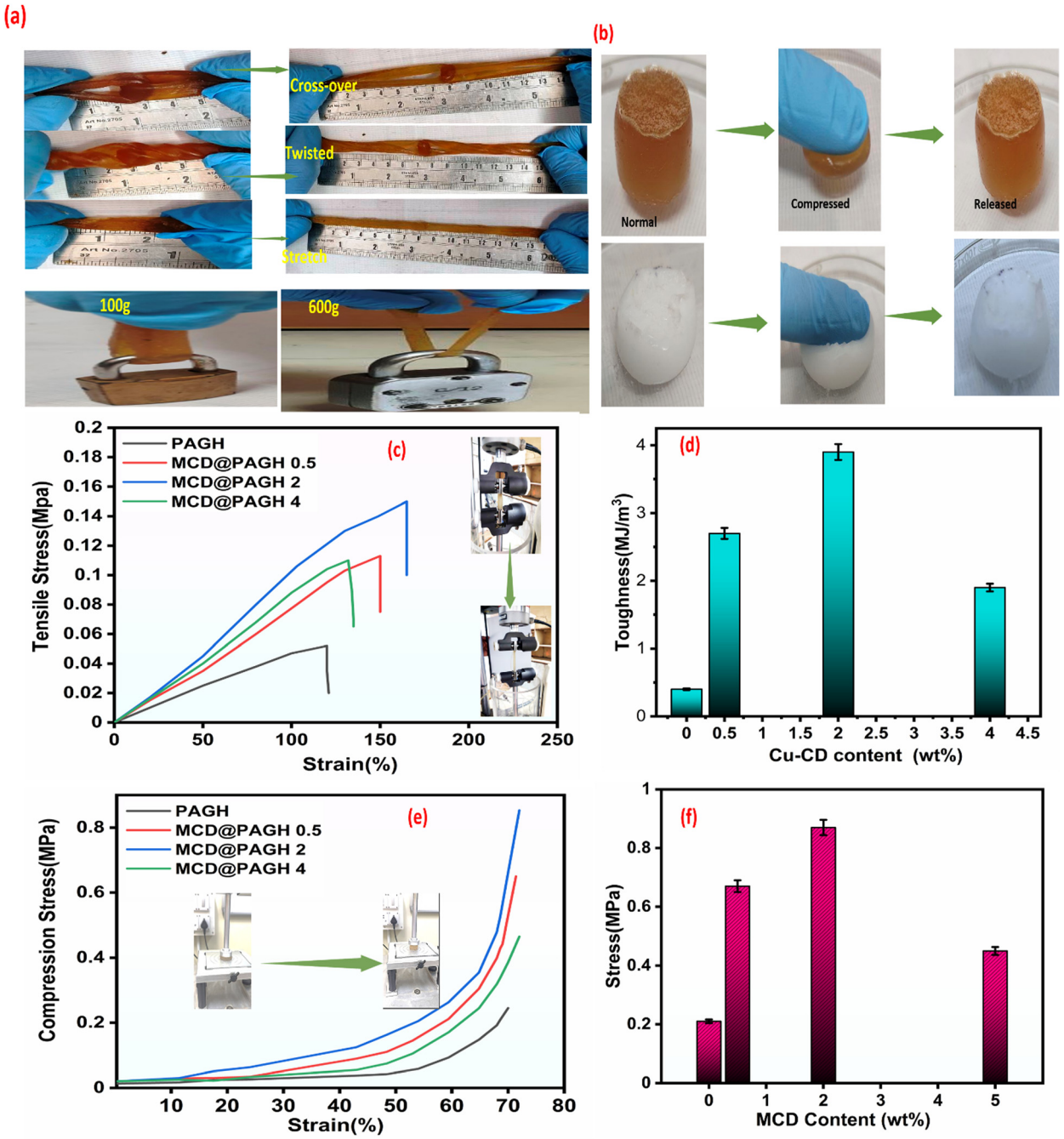

Fig. 2 (a) Photos of the stretching of the MCD@PAGH. (a) Crossover stretching, twisting and stretching between two MCD@PAGH, holding a weight of 100–600 g for the MCD@PAGH. (b) Compression image of MCD@PAGH and PAGH. (c) Tensile stress–strain plot. (d) Toughness of MCD@PAGH with different MCDs wt%. (e) Compressive stress–strain plot. (f) Compressive stress at 73% strain of MCD@PAGH with different MCD wt%.

which tolerate energy absorption and dissipation under loading by the breaking and restoration of bonds.

3.4. Self-healing properties of MCD@PAGH

Self-healing is the ability to retain the initial properties of the material in response to the damage and is an essential characteristic of the wearable patch sensor. To demonstrate the self-healing property, two cylinder-shaped MCD@PAGH samples, one with a colour dye and original MCD@PAGH, were cut in half and then brought into contact at room temperature (Fig. 3a). Within 5 min, the samples were integrated together into a single hydrogel. Surprisingly, the self-healed hydrogel could easily bear the stretching when pulled perpendicularly to the merged surface without forming any crack, which indicates the self-healing nature of the material (Fig. 3b), and the joined rectangular hydrogel strip sample could be freely stretched. For MCD@PAGH 2, the tensile strain after 24 h of damage is 84% of the original MCD@PAGH 2, indicating the complete healing of

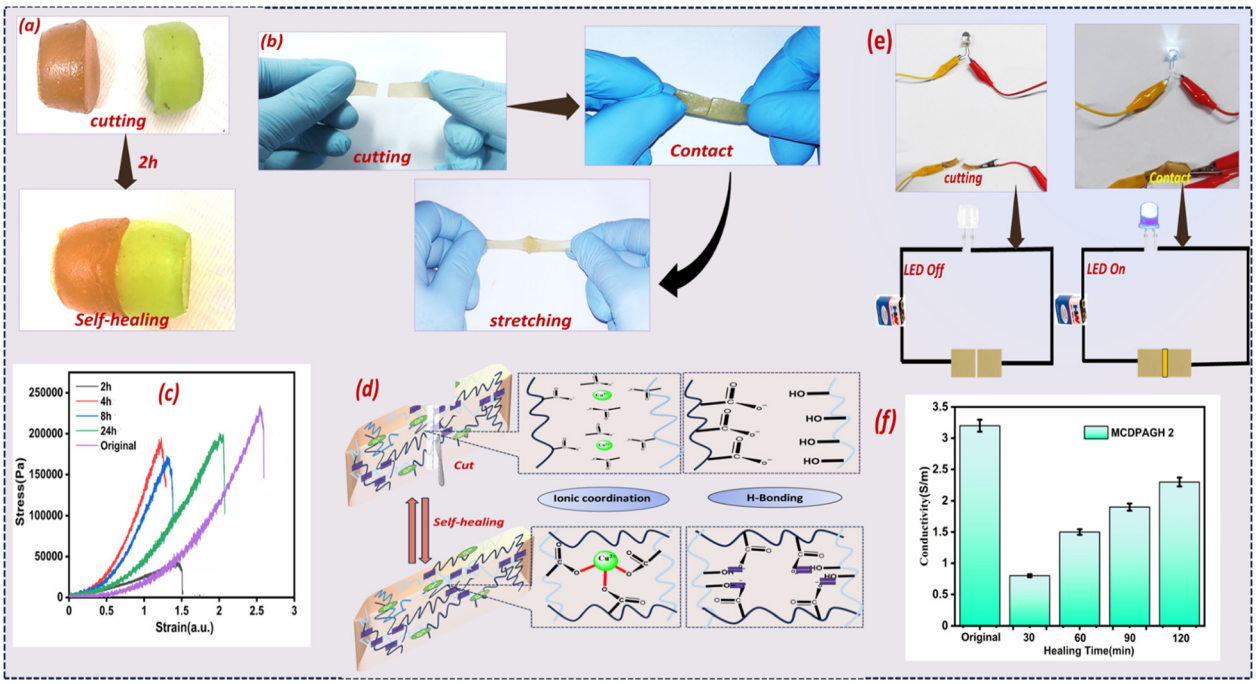

Fig. 3 (a) Self-healing study of MCD@PAGH. (b) Stretching after healing. (c) Stress–strain curve of MCD@PAGH with time interval. (d) Self-healing mechanism. (e) Brightness of LED after healing of the hydrogel. (f) Conductivity of the hydrogel after healing.

the hydrogel (Fig. 3c). The above observations imply that the dynamic interaction and mechanical strength of the hydrogel were restored, and this self-healing behaviour is not due to simple surface adhesion. The strong intramolecular hydrogen

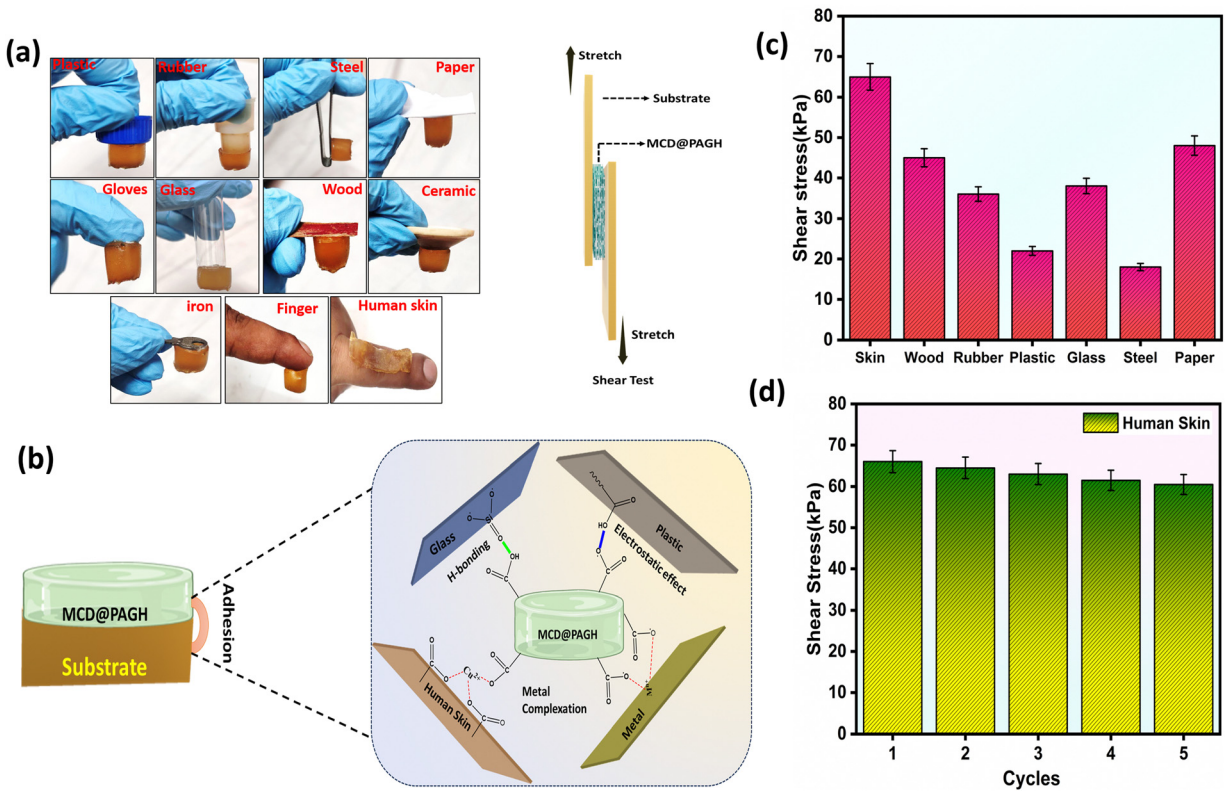

Fig. 4 (a) Pictures of the adhesive properties of MCD@PAGH. (b) Adhesion mechanism of MCD@PAGH to various substrates. (c) Adhesive strength of the MCD@PAGH to various substrates. (d) Cyclic adhesion study of the MCD@PAG to human skin.

bonding and electrostatic interaction, ion coordination bond between hydrophilic functional groups and metal-doped carbon dot surface inside the hydrogel network improves the refurbishment ability of the hydrogel (Fig. 3d). To demonstrate the restoration of the conductive nature of the materials after self-healing, the hydrogel was connected to a circuit with an LED bulb. The LED lightened upon application of power but went out when the gel was cut into two pieces due to the distraction of the conductive path (Fig. 3e). When the hydrogel pieces were brought close to each other, the LED bulb illuminated again just after 2 min. The conductivity of MCD@PAGH 2 hydrogel was 70% restored after 2 h of self-healing (Fig. 3f).

3.5. Adhesive properties of MCD@PAGH

The adhesive property of the prepared MCD@PAGH was examined on different surfaces. As demonstrated in Fig. 4a, MCD@PAGH strongly adheres to plastic, rubber, steel, paper, gloves, glass, wood, ceramic and human skin. The attachment between the hydrogel and metal can be assigned to the formation of the coordination bond between the –OH and –COOH functional groups of the hydrogel and the metal (Fig. 4b).[32] The strong adhesion of MCD@PAGH on human skin can be assigned to the electrostatic interaction and strong H-bond interaction between the protein on the surface of the tissues and the OH/COOH group in the hydrogel.[33] The adhesion strength of hydrogel to human skin was found to be 65 kPa, demonstrating excellent adhesion to the skin (Fig. 4c). It remains above 62.2 kPa (Fig. 4d) even after 5 cyclic applications (Fig. 4d). This slight decrease may be a consequence of the loss of moisture from the surface and interference of dust particles during the repeated adhesion test. More importantly, MCD@PAGH tightly adheres with non-planar human skin and keeps initial conformation intact even after wrist movement. There were no signs of irritation or allergies after peeling off the hydrogel from the skin (Fig. S9a, b and Movie S3, ESI†). With an increase in the MCD content from 0 to 4 mg mL^{-1}, the water swelling percentage was decreased from 990.65% to 645.45%. Moreover, the hydrogel has shown outstanding water absorption speed and reliable water retention performance (Fig. S9c and d, ESI†), which are vital for sweat sampling and storing wearable sensors.

3.6. Cytotoxicity and bacteriostatic activity of MCD@PAGH

We explored the bacteriostatic activity of PAGH as it is an essential requirement for wearable applications.[34] Using PAGH as the control, PAGH with the addition of MCD shows higher bacterial killing efficiency (Fig. 5a). Simultaneously, the survival rate percentage of MCD@PAGH against *S. aureus* and *E. coli* reached 9% and 10%, respectively (Fig. 5b), which confirms that the introduction of MCD effectively endows PAGH with potent antibacterial properties by inhibiting bacterial metabolism.

Good biocompatibility is a notable advantage of biomaterial-based hydrogels, which is particularly beneficial for prolonged

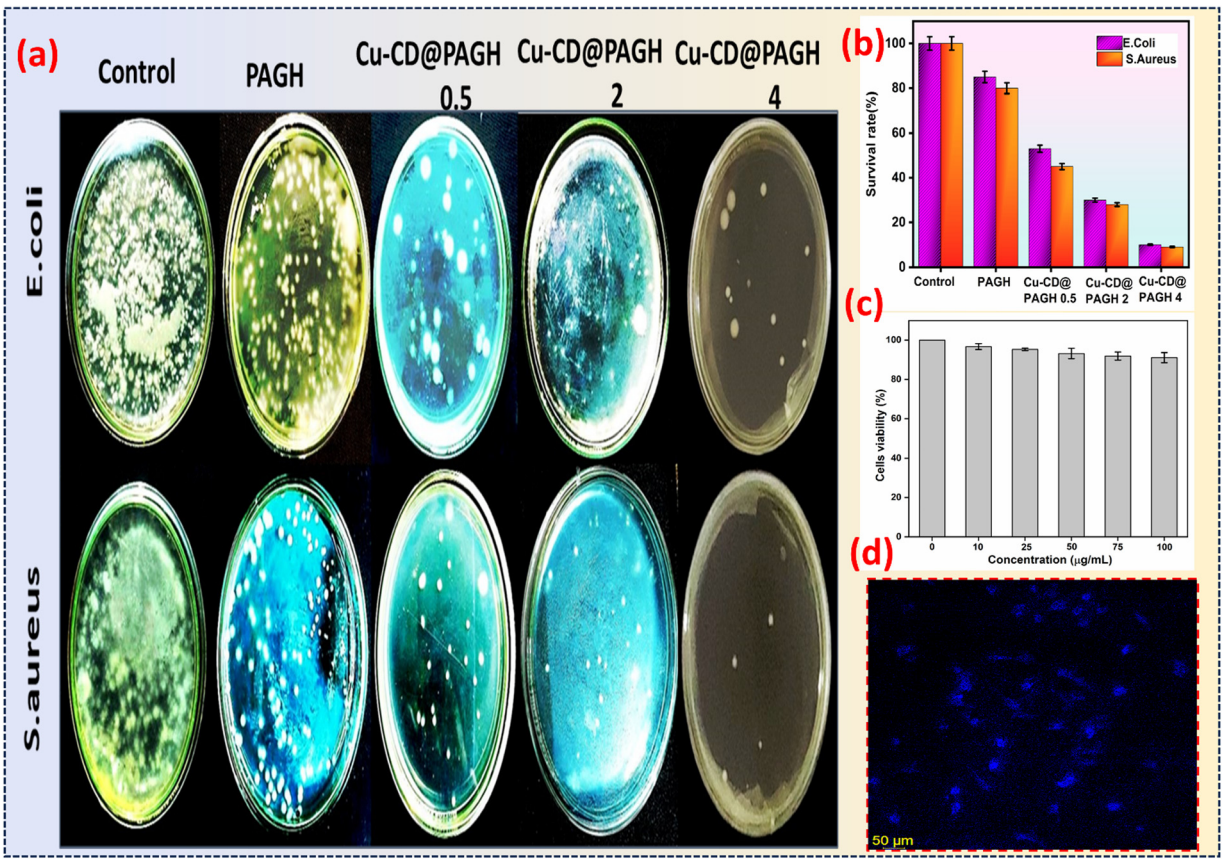

Fig. 5 (a) Antibacterial activity of MCD@PAGH, (b) survival rate of MCD@PAGH, (c) cell viability study of MCD@PAGH, (d) CLSM image of LN229.

contact between the hydrogel and the human body.[35] As shown in Fig. 5c, the nontoxicity of MCD@PAGH to cells was verified by LN229 cell tests. After 24 h of culture with MCD@PAGH extract in the concentration range of 0–100 μg mL^{-1}, the cell viability was observed to be above 91%, confirming the excellent biocompatibility of MCD@PAGH. Simultaneously, live–dead fluorescence staining was conducted on cells cultured with 2 mg mL^{-1} MCD@PAGH extract using the CLSM method. As shown in Fig. 5d, live cells growing adherently to the wall could be observed evenly distributed across the cell culture plate, visually displaying the survival status of the cells, demonstrating that MCD@PAGH has excellent biocompatibility and can be used for health purpose.

3.7. MCD@PAGH patch for monitoring Ca^{2+} through fluorescence

Before proceeding to monitor Ca^{2+} using MCD@PAGH patch, we examined the FL sensitivity of MCD toward Ca^{2+} in solution. We found that the FL intensity of MCD is selectively quenched in the presence of Ca^{2+} in the linear range of 5–300 μM with an LOD (limit of detection) of 47.51 μM (ESI,† Fig. S10). The reason behind the quenching is a possible electron transfer process, as established in Fig. S11 and Scheme S2 (ESI†) (FL lifetime study, DLS (dynamic light scattering), zeta potential, ESI†). To explore the utility of MCD@PAGH as a wearable patch to monitor Ca^{2+} in sweat during daily activities, we investigated the response of MCD@PAGH towards different Ca^{2+} ions in simulated sweat prepared as per the procedure mentioned in ESI.† It was observed that there was a significant quenching in the intensity of emission peak at λ_{445} when the Ca^{2+} concentration was increased linearly from 0 to 150 μM (R^2 = 99, Fig. 6a). The limit of detection was found to be 16.33 μM. The concentration of Ca^{2+} in real sweat varied from 5 μM to 17 μM. Hence, the developed hydrogel film can be applied to monitor Ca^{2+} in human sweat. Originated from the intense luminescence of MCD, MCD@PAGH patch also shows intense blue emission under UV lamp, as mentioned in Fig. 1g. After the dropwise addition of calcium up to a certain concentration, the colour of the hydrogel patch reduced to cyan blue from dark blue, which can be represented in terms of G/B (green/blue) value. The corresponding images are shown in Fig. 6b, and a good linear correlation was established in the concentration range (0–100 μM) with a regression factor R^2 = 0.996. Using RGB app-based analysis, the limit of visual detection of Ca^{2+} in simulated sweat solution was 7.84 μM. Many interfering metabolites and electrolytes such as Na^+, K^+, Mg^{2+}, glucose, lactate, and urea are present in human sweat; the possibility of their influences on the fluorescence response of MCD@PAGH at the same concentrations have been explored. It is clearly seen that other metabolites could not change the fluorescence colour significantly, whereas in the case of Ca^{2+}, the fluorescence of the hydrogel patch is diminished (Fig. 6c). To assess the practical sensing performance of the Ca-responsive hydrogel patch, a disposable first-aid patch was designed by pasting the thin rectangular hydrogel to an adhesive tape and found convenient for wearing on different body parts including joints (Fig. 6d).

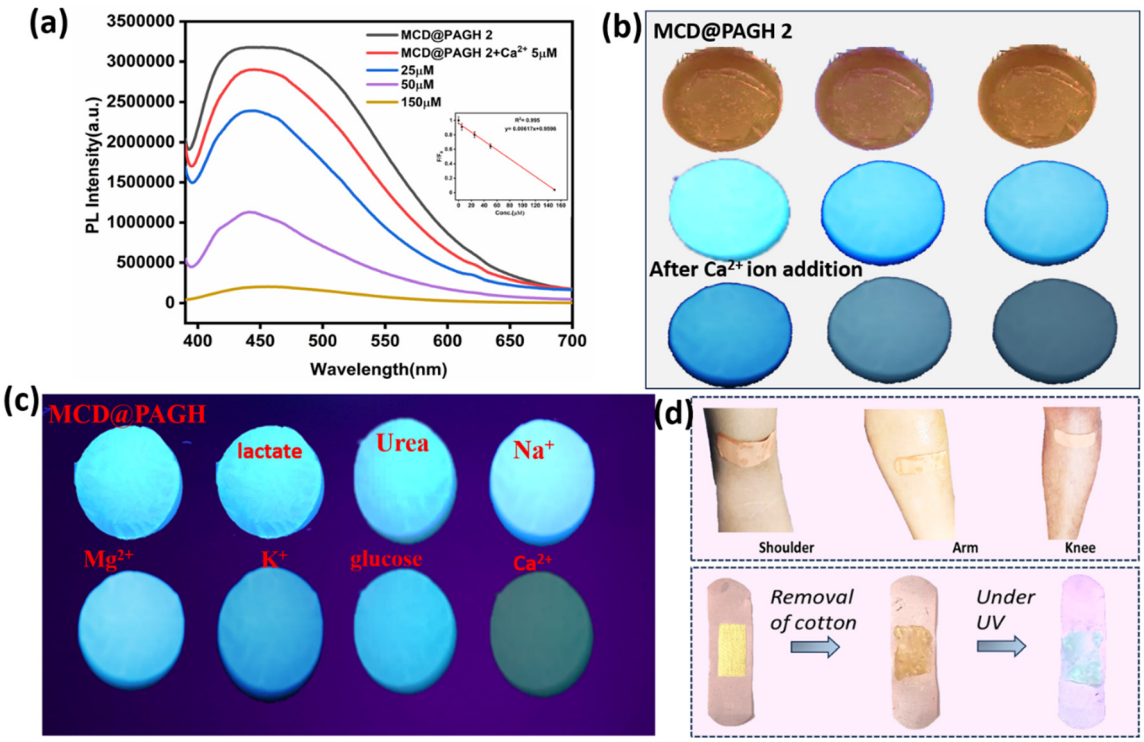

Fig. 6 (a) Hydrogel patch under day light. (b) Ca^{2+} detection in artificial sweat by hydrogel patch under UV (365 nm) light. (c) RGB app-based linear fitting of hydrogel patch. (d) Selectivity study of hydrogel patch compared to other metabolites and ions in sweat. (e) Hydrogel-based band-aid attached to shoulder, arm, knee.

Three types of sweat samples were collected from 3 parts of body, *e.g.*, shoulder, hand and knee, and the Ca^{2+} concentration was measured from the calibration curve obtained from RGB app. It was found that Ca^{2+} concentration in knee, shoulder and hand was 13, 15 and 8 μM, respectively (Fig. S12a–c, ESI†). All these values are within the physiological range of Ca^{2+} ion in the human body, which indicates that the proposed materials could be an easy alternative to monitor the Ca^{2+} concentration as compared to other reported materials on the monitoring of Ca^{2+} ions in human sweat (Table S4, ESI†). Details of the RGB app-based detection and stability of the hydrogel patch are explained in the ESI† (Fig. S13a and b).

3.8. MCD@PAGH patch for the electrochemical monitoring of Ca^{2+}

Owing to the electrical conductance, Ca^{2+} recognition and adhesion properties of MCD@PAGH were explored to assay Ca^{2+} electrochemically. Thus, a piece of the hydrogel was attached with the two electrodes and current responses at variable voltages were recorded. MCD@PAGH shows an initial current of 0.01002 A (at +5 V), which indicates its permeability. After the addition of $CaCl_2$ solution, a remarkable increase in current was observed (Fig. 7a). It was found that MCD@PAGH is sensitive to Ca^{2+} within the concentration range from 1 mM to 1 nM (Fig. 7b). In line with our expectation, the rate of change of current is up to 120% for 1 mM Ca^{2+}, whereas it reduces to 8% for Ca^{2+} for 1 nM of Ca^{2+} concentration. A linear relationship with $R^2 = 0.99$ was obtained from 1×10^{-9} to 1×10^{-3} by plotting current *versus* concentration (Fig. 7c). Moreover, the current response was monitored from different positions of the MCD@PAG sensor patch (Fig. 7d, left) to check the reproducibility of Ca^{2+} response at 1 mM concentration. All the positions of the patch maintain a rate of change of current is >55% (Fig. 7d, right). In contrast, even after soaking the PAGH six times with Ca^{2+}, there was no significant change in the current response (Fig. S14, ESI†). When Ca^{2+} was added to the MCD@PAGH network, the metal ion crosslinks with the –COOH and EDTA groups of MCD, which causes the ion current change. The selectivity of MCD@PAGH was examined by measuring its response towards other cations and anions. With the dropwise addition of cations (*e.g.*, Cu^{2+}, Pb^{+}, Fe^{3+}, Ni^{2+}, Hg^{2+}, Co^{2+}, Al^{3}, Cr^{3+}) and anions (*e.g.*, SO_4^{2-}, HCO_3^{-}, $H_2PO_4^{-}$, NO_3^{-}), the current changes rates were <5% under the similar experimental condition, whereas for Ca^{2+}, the rate is still >50% (Fig. 7e). Therefore, it has been determined that our material exhibits a higher electrochemical Ca^{2+} responsiveness compared to the material mentioned in Table S4 (ESI†). A portable multimeter resistance was employed to observe Ca^{2+} monitoring to the patch (Fig. 7f). MCD@PAGH sliced into a square shape (15 mm in height and 10 mm width) and the patch was placed on the top of the hand to precisely monitor the Ca^{2+} trends in human sweat (Fig. 7g). After running for 30 min, the sweat is absorbed by the patch and the patch is attached with Cu wires applying a two-sided conductive tape to rapidly check the change in resistance within 5 min. Fig. 7h shows the change in resistance induced by sweat. Initially,

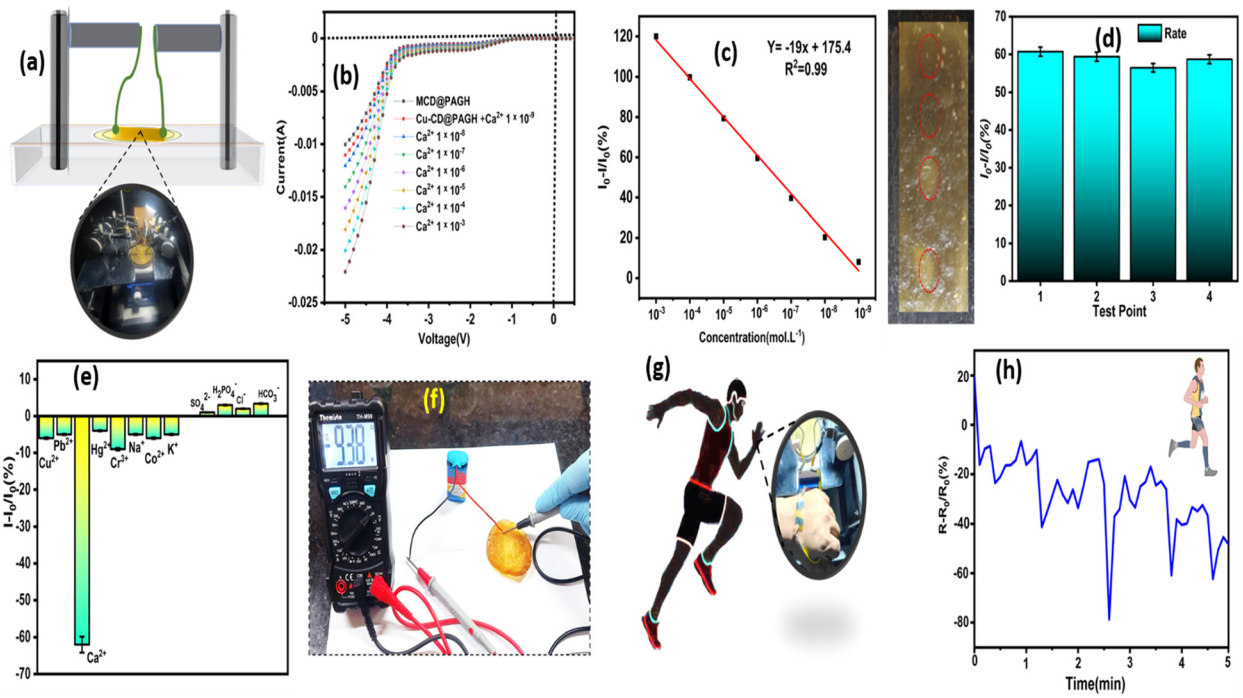

Fig. 7 (a) Schematic of MCD@PAGH as a patch responsive to Ca^{2+}. (b) *I*–*V* plot of the MCD@PAGH patch to various concentrations of Ca^{2+} solution. (c) Linear-fitting plot between current and added Ca^{2+} concentration. (d) Repeatability study of MCD@PAGH response to Ca^{2+}. (e) Selectivity study of MCD@PAGH towards different cations and anions. (f) Picture of the hydrogel patch attached to a multimeter. (g) Patch placed on the top of the hand while running. (h) Change in the rate of resistance for Ca^{2+} in human sweat during running.

during the first 2 minutes, the running speed remained relatively constant. However, as the running speed increases, the sweat volume in the body rapidly increases, which may lead to a gradual increase in resistivity. In the last 2 minutes, the running pace slowed down and the resistivity gradually decreased, confirming a lower concentration of Ca^{2+} in the sweat.

4. Conclusion

In conclusion, we have synthesized a conductive skin adhesive patch by embedding copper-doped carbon dot in a PVA–agar hydrogel. The combination of PVA : agar : carbon dot (MCD) in (4 : 1 : 0.12) weight percentage induced multiple hydrogen bonding and coordination bonds, which results in excellent stretchability with a tensile stress of 0.149 MPa and 164% strain. The uniform distribution of MCD nanoparticles in PVA–agar creates inter-connected conductive channels that confer electrical conductivity to the hydrogel. The fluorescence emission of MCD and inherent Ca^{2+} specificity of MCD enables the MCD@PAG patch to recognize the level of Ca^{2+} in sweat by both electrochemical and fluorescence measurements when applied as a wearable skin. Compared to the reported wearable electronic-skin Ca sensors, the developed MCD@PAG patch sensor addressed vital challenges such as high stress–strain, electrical conductivity, antimicrobial, biocompatibility, adhesive and self-healing properties, which could be further optimized to design soft materials.

Data availability

All data will be available on request.

Conflicts of interest

There are no conflicts to declare.

Acknowledgements

This work is financially supported by SERB, DST, Govt. of India (CRG/2018/001717). LB thanks NIT Rourkela for providing doctoral research fellowship.

References

1 I. You, K. K. R. Choo and L. C. Ho, *Comput. Electr. Eng.*, 2018, **65**, 376–392.
2 G. Xiu, C. Cheng, W. Yuan, Z. Liu, L. Zhu, X. Li and Q. Liu, *Sens. Actuators, B*, 2019, **297**, 126743.
3 W. Wang, Y. Chen, C. Xiao, S. Xiao, C. Wang, Q. Nie and Y. Lu, *Chem. Eng. J.*, 2023, **474**, 145953.
4 A. J. Bandodkar and J. Wang, *Trends Biotechnols*, 2014, **32**, 363–371.
5 P. Kakria, K. N. Tripathi and P. Kitipawang, *Int. J. Telemed. Appl.*, 2015, **1**, 373474.
6 B. L. Baker, Physiology of sweat gland function, *Temperature*, 2019, **6**, 211–259.
7 Y. L. Chen, W. H. Kuan and C. L. Liu, *Int. J. Environ. Res. Public Health*, 2020, **17**, 3377.
8 Y. Lin, Y. Zheng, Y. Guo, Y. Yang, H. Li, Y. Fang and C. Wang, *Sens. Actuators, B*, 2018, **273**, 1654–1659.
9 W. G. Cho, F. Altamirano and A. J. Hill, *Biochim. Biophys. Acta, Mol. Basis Dis.*, 2016, **1862**, 763–777.
10 H. Y. Y. Nyein, W. Gao, Z. Shahpar, S. Emaminejad, S. Challa, K. Chen and A. Javey, *ACS Nano*, 2016, **10**, 7216–7224.
11 G. Su, N. Wang, Y. Liu, R. Zhang, Z. Li, Y. Deng and B. Tang, *Adv. Mater.*, 2024, 2400085.
12 D. Liu, C. Huyan, Z. Wang, Z. Guo, X. Zhang, H. Torun and F. Chen, *Mater. Horiz.*, 2023, **10**, 2800–2823.
13 A. Shit, N. N. Giang and S. Y. Park, *Compos. Sci. Technol.*, 2022, **218**, 109212.
14 K. S. Kailasa, J. D. Joshi, R. M. Kateshiya, R. J. Koduru and N. I. Malek, *Mater. Today Chem.*, 2023, **23**, 100746.
15 F. Q. Li, X. Chen, H. Wang, M. Liu and H. L. Peng, *ACS Appl. Mater. Interfaces*, 2022, **15**(10), 13290–13298.
16 L. Wang, T. Xu, X. He and X. Zhang, *J. Mater. Chem. C*, 2021, **9**, 14938–14945.
17 Q. Li, C. He, C. Wang, Y. Huang, J. Yu, C. Wang and G. Qing, *Small*, 2023, **19**, 2207932.
18 Z. Sun, C. Dong, B. Chen, W. Li, H. Hu, J. Zhou and Z. Huang, *Small*, 2023, **9**, 2303612.
19 X. Sun, C. Luo and F. Luo, *Eur. Polym. J.*, 2020, **124**, 109465.
20 C. Cheng, X. Peng, L. Xi, C. Wan, S. Shi, Y. Wang and X. Yu, *Food Funct.*, 2022, **13**, 9622–9634.
21 L. Behera, L. Mishra, M. Mishra and S. Mohapatra, *J. Mater. Chem. B*, 2024, **12**, 5181–5193.
22 J. Cao, Y. Cai, L. Yu and J. Zhou, *J. Mater. Chem. B*, 2019, **7**, 676–683.
23 B. C. Pattnayak and S. Mohapatra, *J. Environ. Chem. Eng.*, 2022, **10**(6), 108616.
24 W. Li, Z. Wu, J. Zhao, M. Jiang, L. Yuan, Y. Guo and R. Cai, *Int. J. Biol. Macromol.*, 2023, **247**, 125652.
25 J. Jiang, X. Liu, J. Han, K. Hu and J. S. Chen, *Processes*, 2021, **9**, 680.
26 A. Zhang, W. Zheng, Z. Yuan, J. Tian, L. Yue, R. Zheng and J. Liu, *Chem. Eng. J.*, 2020, **380**, 122486.
27 L. Behera, D. Pati, B. B. Sahu and S. Mohapatra, *Colloids Surf., A*, 2022, **653**, 130002.
28 B. Barik, L. Behera and S. Mohapatra, *Ind. Eng. Chem. Res.*, 2023, **62**, 10849–10860.
29 Y. Yang, C. Wang, Q. Shu, N. Xu, S. Qi, S. Zhuo and J. Du, *Spectrochim. Acta, Part A*, 2022, **268**, 120681.
30 Z. Qin, X. Sun, Q. Yu, H. Zhang, X. Wu, M. Yao and J. Li, *ACS Appl. Mater. Interfaces*, 2020, **12**, 4944–4953.
31 R. S. Shin, M. S. Jung, M. Zalabany, K. Kim, P. Zorlutuna, S. Kim and B. Khademhosseini, *ACS Nano*, 2013, **7**, 2369–2380.
32 F. Lin, Z. Wang, Y. Shen, L. Tang, P. Zhang, Y. Wang and B. Lu, *J. Mater. Chem. A*, 2019, **7**, 26442–26455.
33 Z. Ren, T. Ke, Q. Ling, L. Zhao and H. Gu, *Carbohydr. Polym.*, 2021, **273**, 118533.
34 D. Tahtat, M. Mahlous, S. Benamer, A. N. Khodja, S. Larbi Youcef, N. Hadjarab and W. Mezaache, *J. Mater. Sci.: Mater. Med.*, 2011, **22**, 2505–2512.
35 H. Cheng, R. Devi Keerthika, Y. K. Huang, M. Ganesan, K. S. Ravi and C. C. Lin, *Small*, 2024, 2401201.